Charge transfer and antiferromagnetic order in the *A*-site-ordered perovskite $LaCu_3Fe_4O_{12}$

Wei-tin Chen,*[ab] Youwen Long,†[a] Takashi Saito,[a] J. Paul Attfield[b] and Yuichi Shimakawa[a]

Received 19th March 2010, Accepted 21st May 2010
DOI: 10.1039/c0jm00767f

High resolution neutron powder diffraction has been used to study the charge states and spin order in the *A*-site-ordered perovskite $LaCu_3Fe_4O_{12}$. This undergoes a first-order phase transition between cubic *Im*-3 structures with charge distributions $LaCu^{3+}{}_3Fe^{3+}{}_4O_{12}$ and $LaCu^{2+}{}_3Fe^{3.75+}{}_4O_{12}$ at $T_{CT} \approx 400$ K. Bond valence sums confirm that these charge states are adopted in the two phases, and there are no substantial valence fluctuations near the charge transfer transition. G-type antiferromagnetic order of *B*-site Fe^{3+} spins is observed in the low temperature phase $LaCu^{3+}{}_3Fe^{3+}{}_4O_{12}$ and the ordered moment at 50 K is 4.0 μ_B. Magnetic moment is absent at the *A*′-site Cu^{3+} cation. The thermal evolution of the ordered moment enables an intrinsic $T_{N'} \approx 600$ K to be estimated, although the actual upper limit for the spin order is T_{CT}. No long range magnetic ordering was found in the high temperature phase, $LaCu^{2+}{}_3Fe^{3.75+}{}_4O_{12}$, showing that any ordering transition for this regime has $T_M < T_{CT}$.

1. Introduction

A-site-ordered double perovskite oxides with the general formula $AA'_3B_4O_{12}$ have attracted much interest owing to their wide variety of physical properties.[1–4] In these materials, the *A* and *A*′ cations are 1 : 3 ordered at the *A* site in the simple ABO_3 structure, resulting in a framework consisting of heavily tilted BO_6 octahedra and $A'O_4$ squares. Unlike the *A* site in simple perovskite oxides, which is usually occupied by alkali, alkaline earth, or rare earth cations, the *A*′ site can accommodate transition metal cations, such as Cu^{2+} and Mn^{3+}, which are Jahn–Teller-active. Therefore, *A*′-*A*′ and/or *A*′-*B* interactions may give rise to novel physical properties in addition to the usual *B*-*B* interactions. For example, antiferromagnetic couplings between the *A*′-site Cu spins and the *B*-site Mn spins produce spin-polarized conduction carriers in $La/BiCu_3Mn_4O_{12}$, which cause colossal magnetoresistance under weak magnetic fields.[5–7] Heavy-Fermion-like transport properties observed in $CaCu_3Ru_4O_{12}$ are also attributed to the interaction between the *A*′-site Cu spins and the *B*-site Ru itinerant electrons.[8–10]

Recently we found another notable example of *A*′–*B* interaction in $LaCu_3Fe_4O_{12}$, which is a temperature-induced intersite charge transfer.[11] High-pressure conditions are required for the synthesis of the compound, in which the unusually high valent Cu^{3+} and $Fe^{3.75+}$ cations are stabilized in this *A*-site-ordered structure. Because of the delicate balance between the two charge states, the high-temperature (HT) charge distribution $LaCu^{2+}{}_3Fe^{3.75+}{}_4O_{12}$ changes to a low-temperature (LT) distribution $LaCu^{3+}{}_3Fe^{3+}{}_4O_{12}$ at $T_{CT} = 393$ K on cooling. Simultaneous valence changes at the *A*′ and *B* sites result from the charge transfer $3Cu^{2+} + 4Fe^{3.75+} \rightarrow 3Cu^{3+} + 4Fe^{3+}$ where the paramagnetic metallic phase at high temperature transforms to the antiferromagnetically-ordered insulating phase at low temperature. A similar charge transfer was also observed in the isostructural compound $BiCu_3Fe_4O_{12}$ at 428 K.[12]

Such drastic changes in the physical properties of transition metal oxides usually require doping or the application of high pressures, so the spontaneous intersite charge transfer transition in $LaCu_3Fe_4O_{12}$ provides a remarkable example of switching charge and spin states in an oxide material. To confirm the distribution of charge states and to determine the spin order in the LT phase, we have carried out a neutron powder diffraction (NPD) study of $LaCu_3Fe_4O_{12}$ for which the results are reported here.

2. Experimental

A polycrystalline $LaCu_3Fe_4O_{12}$ sample was prepared with a high-pressure and high-temperature synthesis technique as described by Long *et al.*[11] The stoichiometric amounts of La_2O_3, CuO, and Fe_2O_3 with a $KClO_4$ oxidizing agent were placed in a platinum capsule as starting materials. The mixture was then treated at 10 GPa and 1400 K for 1 h with a cubic-anvil-type high pressure apparatus. After treatment, the sample was quenched to room temperature before the pressure was released. The accompanying KCl and by-products were washed out with a dilute acid solution. The obtained compound was confirmed to crystallize in a $2a_0 \times 2a_0 \times 2a_0$ (a_0 represents the lattice parameter in a simple perovskite ABO_3 ~4 Å) *A*-site-ordered double perovskite structure. The charge-transfer transition of the sample at 393 K was confirmed by magnetism and resistivity measurements.[11]

Neutron diffraction data from a ~0.5 g polycrystalline powder sample in a 5 mm-diameter vanadium can were collected using the Super-D2B diffractometer at the Institut Laue-Langevin (ILL), Grenoble, France. The diffraction patterns were recorded in the angular range $5° \leq 2\theta \leq 155°$ with a neutron wavelength of 1.594 Å. The measurements were performed from 50 to 425 K

[a]*Institute for Chemical Research, Kyoto University, Uji, Kyoto, 611-0011, Japan. E-mail: W.Chen@kt8.ecs.kyoto-u.ac.jp*
[b]*Centre for Science at Extreme Conditions (CSEC) and School of Chemistry, The University of Edinburgh, Edinburgh, EH9 3JZ, United Kingdom*
† Present address: Multiferroics Project, ERATO, JST, c/o Cross-Correlated Materials Research Group, FRS, RIKEN, Wako, Saitama 351-0198, Japan.

and the data were collected for 5 h at 50, 300 and 425 K and 3 h at other temperature points. Although the measurements were done with an evacuated container, no effect from the atmosphere in the measured temperature range was confirmed from the reproducibility of the data. The crystal and magnetic structures were analyzed from the diffraction data with the Rietveld method using the General Structure Analysis System (GSAS) software package.[13-14]

3. Results and discussion

3.1. Crystal structure

$LaCu_3Fe_4O_{12}$ was found to be cubic throughout the 50–425 K range and the structure analyses are presented in order of decreasing temperature. The diffraction peaks obtained at 425 K, originating from the HT phase, were well-indexed with the *Im*-3 (No. 204) space group with lattice parameter $a = 7.4140(1)$ Å, and atom positions La 2*a* (0, 0, 0), Cu 6*b* (0, ½, ½), Fe 8*c* (¼, ¼, ¼) and O 24*g* (0.3063, 0.1741, 0) were used as a starting model. The contribution from a small amount of Fe_2O_3 impurity was also fitted in the refinements. The apparent amount (4.2 wt%) is greater than the 2.3 wt% estimated by fitting X-ray data—this may result from significant microabsorption as La and Cu are more neutron absorbing than Fe and O. Due to the high oxygen sensitivity provided by the neutrons, more accurate information on the occupation and positional parameters of oxygen atoms were obtained from the structure analysis. No oxygen deficiency was observed within a deviation of ~0.5% from the occupancy refinement, so the composition was fixed at the stoichiometric value. A satisfactory fit was achieved with fitting residuals $R_{wp} = 5.12\%$ and $\chi^2 = 2.95$, as shown in Fig. 1 (a), and the structural parameters, selected bond distances and angles are listed in Table 1.

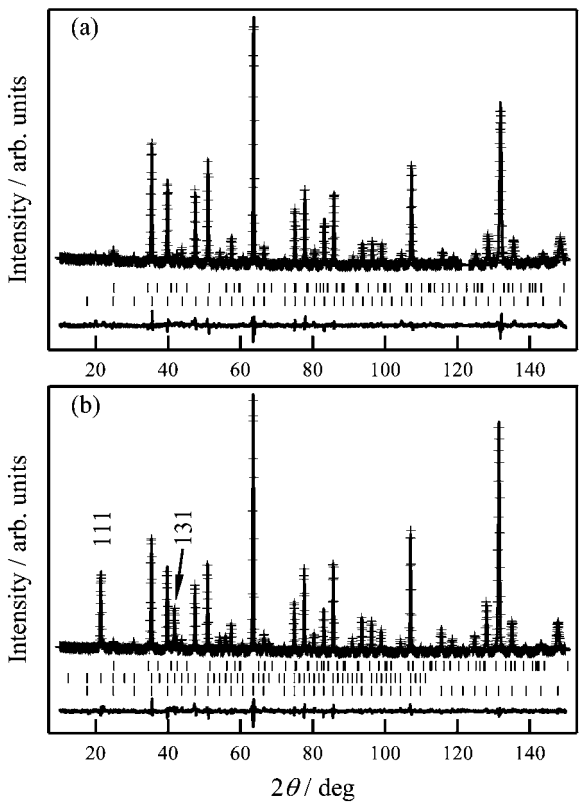

Fig. 1 Neutron diffraction patterns of $LaCu_3Fe_4O_{12}$ at (a) 425 K where bottom and top reflection markers are respectively for $LaCu_3Fe_4O_{12}$ and 4.2 wt% of Fe_2O_3, (b) 50 K, with the principally magnetic 111 and 131 reflections labeled, and Bragg markers for the nuclear and magnetic phases of $LaCu_3Fe_4O_{12}$ and Fe_2O_3 from bottom to top. Instrumental scatter at ~120° is excluded from the refinements.

The $A'O_{12}$ polyhedron is highly distorted and consists of three sets of A'–O distances, with the four short Cu–O distances of 1.931(2) Å defining a square-plane. The bond valence sum[15] (BVS) estimate for the A'-site Cu charge was +2.08, in good agreement with the ideal Cu^{2+} state. The Fe–O bond lengths in the *B*-site octahedra were 1.9814(6) Å, and the BVS value was calculated to be +3.41. This is within an acceptable difference (9%) from the ideal value of +3.75. Hence, this refinement confirms the stoichiometric nature of the material and the ideal $LaCu^{2+}{}_3Fe^{3.75+}{}_4O_{12}$ charge distribution in the HT phase.

Phase coexistence was observed at 400 K, where a two-phase refinement showed 82.3 and 17.7% of the HT and LT phases, respectively. This confirms the suggested first-order nature of the phase transition.[11] The difference in volume between the HT and LT phases reaches 1.3% (Fig. 2 (a)) at this temperature. At 300 K and lower temperatures, a single LT phase was observed and is also described by an *Im*-3 model. Magnetic intensities were observed in this regime (see the next section) but no further peak splittings or superlattice peaks were observed. Good fits were achieved with $R_{wp} = 5.15\%$ and $\chi^2 = 1.98$ for the 300 K data shown in Fig. 1 (b), and the structural information is listed in Table 1. The Cu–O bond distances decrease by 2.4% to 1.885(2) Å from those of the HT phase. As a result, the BVS increases to +2.95, revealing a pure Cu^{3+} state in the LT phase. The Fe–O bonds, on the other hand, increase in length to 2.0059(7) Å, giving a BVS value of +3.01 for Fe. These results confirm that the LT charge composition is $LaCu^{3+}{}_3Fe^{3+}{}_4O_{12}$ with no evidence for mixed Cu or Fe valences. Hence the charge state changes $3Cu^{2+} - 3e^- \rightarrow 3Cu^{3+}$ and $4Fe^{3.75+} + 3e^- \rightarrow 4Fe^{3+}$ occur completely and simultaneously at the charge transfer transition in $LaCu_3Fe_4O_{12}$. The Cu–O–Fe and Fe–O–Fe angles at 300 K are 111.64(5) and 135.8(1)°, respectively. Although the Fe–O–Fe tilting angle decreases through the transition, the considerable elongation in the Fe–O bond lengths increases the volume of FeO_6 octahedra, which dominate the cell volume change resulting in a significant volume increase on going from the HT to the LT phase.

In the LT regime, the BVS's for both A'-site Cu and *B*-site Fe are close to +3, and neither significant electronic changes nor critical fluctuations of Cu and Fe charge states are observed, as shown in Table 1 and Fig. 2 (b). No evidence of Fe charge disproportionation is found down to 50 K, which is in contrast to $CaCu^{2+}{}_3(Fe^{3+}{}_2Fe^{5+}{}_2)O_{12}$ where a $2Fe^{4+} \rightarrow Fe^{3+} + Fe^{5+}$ disproportionation occurs at 210 K.[16] Both the $Fe^{3.75+}$ state in the HT phase and the Cu^{3+} state in the LT phase are unusually high and the energy levels between these two states should be comparable and competing. However, the isostructural phase transition with the intersite charge transfer, instead of charge disproportionation, resolves the instability of the high oxidation state of the *B*-site $Fe^{3.75+}$ and produces the unusual Cu^{3+} state at the A'-site in

Table 1 Refinement results from Rietveld fits of the $LaCu_3Fe_4O_{12}$ structure to powder neutron diffraction data. The lattice parameter, cell volume, isotropic thermal factor, atomic coordinations, ordered magnetic moment, selected bond distances, bond angles, BVS results, and reliability factors from the refinements are listed.

		HT Phase[a]		LT Phase[a]								
Temperature/K		425	400[b]	400[b]	375	350	325	300	275	200	125	50
a/Å		7.4140(1)	7.4109(2)	7.4443(2)	7.4391(1)	7.4378(2)	7.4365(1)	7.4351(1)	7.4336(2)	7.4302(1)	7.4274(1)	7.4262(1)
Volume/Å^3		407.53(2)	407.01(3)	412.55(3)	411.68(2)	411.46(3)	411.25(2)	411.02(2)	410.77(3)	410.20(2)	409.75(2)	409.55(2)
La	U_{iso}/Å^2	0.001(1)	0.002(1)	0.003(1)	0.006(1)	0.005(1)	0.006(1)	0.005(1)	0.006(1)	0.002(1)	0.004(1)	0.0021(9)
Cu	U_{iso}/Å^2	0.0164(6)	0.0157(7)	0.0165(7)	0.0127(6)	0.0136(6)	0.0117(6)	0.0119(6)	0.0113(6)	0.0116(6)	0.0094(5)	0.0103(5)
Fe	U_{iso}/Å^2	0.0091(3)	0.0091(3)	0.0092(3)	0.0093(3)	0.0076(3)	0.0081(3)	0.0079(3)	0.0080(4)	0.0063(3)	0.0059(3)	0.0054(2)
	M_z/μ_B	–	–	3.11(9)	3.28(3)	3.44(3)	3.53(3)	3.64(3)	3.70(3)	3.90(3)	4.00(3)	4.03(2)
O	*x*	0.3063(2)	0.3070(3)	0.3100(9)	0.3113(2)	0.3112(2)	0.3115(2)	0.3110(2)	0.3110(3)	0.3112(2)	0.3116(2)	0.3110(2)
	y	0.1741(3)	0.1745(3)	0.1700(9)	0.1695(3)	0.1690(3)	0.1692(3)	0.1690(3)	0.1694(3)	0.1694(3)	0.1690(3)	0.1692(2)
	U_{iso}/Å^2	0.0113(3)	0.0112(3)	0.0113(3)	0.0095(3)	0.0088(3)	0.0083(3)	0.0080(3)	0.0077(3)	0.0066(3)	0.0058(3)	0.0059(2)
La–O/Å × 12		2.612(2)	2.617(2)	2.632(6)	2.637(2)	2.634(2)	2.636(2)	2.632(2)	2.632(2)	2.633(2)	2.633(2)	2.630(2)
Cu–O/Å × 4		1.931(2)	1.928(2)	1.898(7)	1.887(2)	1.885(2)	1.884(2)	1.885(2)	1.887(2)	1.885(2)	1.880(2)	1.884(2)
Fe–O/Å × 6		1.9814(6)	1.9809(7)	2.004(3)	2.0063(7)	2.0068(7)	2.0065(7)	2.0059(7)	2.0046(8)	2.0040(7)	2.0048(7)	2.0029(6)
Cu–O–Fe/°		110.27(4)	110.33(5)	111.4(2)	111.63(5)	111.66(5)	111.69(5)	111.64(5)	111.59(5)	111.62(5)	111.73(5)	111.61(4)
Fe–O–Fe/°		138.6(1)	138.5(1)	136.4(4)	135.9(1)	135.8(1)	135.8(1)	135.8(1)	136.0(1)	135.9(1)	135.7(1)	135.9(1)
BVS (Cu) [c]		2.08	2.09	2.88	2.94	2.95	2.96	2.95	2.94	2.96	2.99	2.96
BVS (Fe) [c]		3.41	3.41	3.01	3.01	3.01	3.01	3.01	3.02	3.03	3.02	3.04
R_{WP} (%)		5.12	5.37	5.37	5.54	6.13	6.09	5.15	7.73	5.97	6.05	5.23
χ^2		2.95	2.29	2.29	2.48	2.29	2.32	1.98	1.55	2.27	2.34	3.27

[a] For the crystal structural refinements, both high- and low-temperature phases adopt cubic space group *Im*-3 (No, 204), where the atomic positions are La 2*a* (0, 0, 0), Cu 6*b* (0, ½, ½), Fe 8*c* (¼, ¼, ¼) and O 24*g* (*x*, *y*, 0). [b] Two-phase refinement was carried out for the 400 K data, which contains 82.3% of the high-temperature phase. [c] The bond valences V_i are estimated from the formula $V_i = \sum\exp[(r_0\text{-}r_i)/b]$, where r_i are the observed M–O distances, and *b* is a typical constant 0.37 Å. The corresponding tabulated empirical r_0 values were used as followed: 1.649 for Cu^{2+}, 1.739 for Cu^{3+} and 1.751 for Fe^{3+}; it should be noted that no r_0 value is listed for mixed-valent cations, therefore for estimation of $Fe^{3.75+}$ the r_0 of Fe^{4+} 1.772 was used.[17]

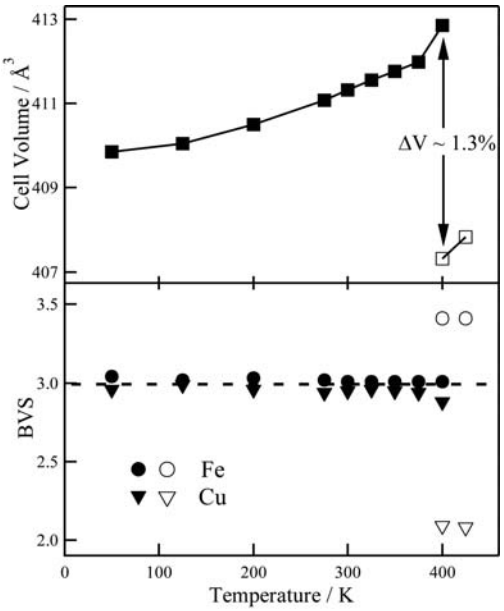

Fig. 2 Temperature dependence of (a) sample volume and (b) BVS values of Fe and Cu ions in $LaCu_3Fe_4O_{12}$, represented by the circle and triangle markers, respectively. The filled and open markers represent the low- and high-temperature phases, respectively, and these coexist at 400 K.

square-planar coordination. This is probably related to the fractional +3.75 state of Fe, which is difficult to accommodate as a simple rock-salt type ordering of the disproportionated Fe^{3+} and Fe^{5+} ions, owing to the requirement of a substantial increase in the lattice energy to accommodate the complex $8Fe^{3.75+} \rightarrow 5Fe^{3+} + 3Fe^{5+}$ charge disproportionation.

3.2. Magnetic structure

As mentioned above, magnetic contributions were observed in addition to the nuclear peaks in the diffraction intensities below the transition temperature. Representative low-angle magnetic Bragg reflections from the 111 and 131 planes at 50 K are clearly seen in Fig. 1 (b), while no magnetic ordering is observed in the HT phase as shown in Fig. 1 (a). The refinements revealed a magnetic superstructure with a (½ ½ ½) propagation vector of the cubic cell. This corresponds to a G-type antiferromagnetic ordering (Fig. 3) where each *B*-site moment is antiparallel to the six nearest neighbors. The refined magnetic moment at the *B* site at 50 K was 4.03(2) μ_B, slightly reduced from the ideal value of 5 μ_B for high spin Fe^{3+} ($3d^5$ $S = 5/2$) due to zero-point and covalency effects. Magnetic moments at the *A*′ site were also examined with various ordering models. However, all refinements resulted in poor fit and no convincing *A*′-site moment was achieved. Therefore, we conclude that the Cu cation at the square-planar-coordinated 6*c* site produces no magnetic contribution. This is consistent with the Cu^{3+} ($3d^8$) valence state with a proposed low spin $S = 0$ configuration, due to considerable energy splitting between $d_{3z^2-r^2}$ and $d_{x^2-y^2}$ orbitals. Such square-planner coordinated trivalent copper cations can also been found in $MCuO_2$ (M = Li, Na, K), which behave as diamagnets.[18–20] It should be noted that the unusual Cu^{3+} might be better described as a $d^9\underline{L}$ configuration, due to its low-lying *d* level with a covalent electronic state and a ligand hole $\underline{L}$.[21] This $d^9\underline{L}$ configuration is known to form singlet between the cation and the ligand (Zang–Rice singlet, as seen in $CaCu_3Co_4O_{12}$ and $YCu_3Co_4O_{12}$),[22] in which the cation shows nonmagnetic behavior as well.

As shown in Table 1 and Fig. 3, the ordered component of the *B*-site magnetic moment decreases gradually with increasing temperature, reaching 3.11(9) μ_B at 400 K where the charge transfer phase transition occurs. Comparison of the thermal evolutions of the Fe charge state (Fig. 2 (b)) and ordered moment (Fig. 3) shows that the Fe spin fluctuations do not result from valence fluctuations as the charge transfer transition is approached. Instead they reflect the intrinsic strength of the spin–spin interactions that would determine the Néel transition temperature if the charge transfer to the HT state did not occur. By fitting an $S = 5/2$ Brillouin function to the moments (Fig. 3), we can estimate the projected Néel temperature T_N' to be ~600 K, whereas the actual $T_N = T_{CT} = 393$ K as the charge transfer drives the change from an antiferromagnetic to a paramagnetic state.

In the $LaCu^{3+}{}_3Fe^{3+}{}_4O_{12}$ LT phase, the Fe^{3+}–O–Fe^{3+} superexchange interaction is dominant, giving rise to G-type antiferromagnetic ordering of Fe spins. (This is in contrast to $CaCu_3Fe_4O_{12}$, which consists of ferromagnetically coupled *B*-site Fe^{3+} and Fe^{5+} spins below the transition.[16]) As the Cu^{3+} cations are non-magnetic, the Fe^{3+} magnetic sublattice in LT $LaCu_3Fe_4O_{12}$ is comparable to that in rare earth (*R*) orthoferrite perovskites $RFe^{3+}O_3$. The series R = La to Lu exhibits antiferromagnetic ordering owing to the Fe^{3+}–O–Fe^{3+} superexchange interactions, where the magnetic transition temperature T_N correlates with the Fe–O–Fe bond angle ϕ.[24-25] The angles decrease from 157 to 141° for $LaFeO_3$ to $LuFeO_3$, leading to the decline of T_N from 750 to 640 K, respectively. From extrapolation of this trend, the LT $LaCu^{3+}{}_3Fe^{3+}{}_4O_{12}$ with the angle ϕ = 136° is predicted to have T_N' ~570 K, which is close to the T_N' value of ~600 K obtained from fitting the $S = 5/2$ Brillouin function to the ordered moment (Fig. 3). These results demonstrate that the spin and charge transfer degrees of freedom in $LaCu_3Fe_4O_{12}$ are decoupled, and that the intrinsic magnetic exchange integral $J_{Fe^{3+}–O–Fe^{3+}}$ ($\sim k_B T_N'$) is significantly larger than the apparent magnitude of $\sim k_B T_{CT}$.

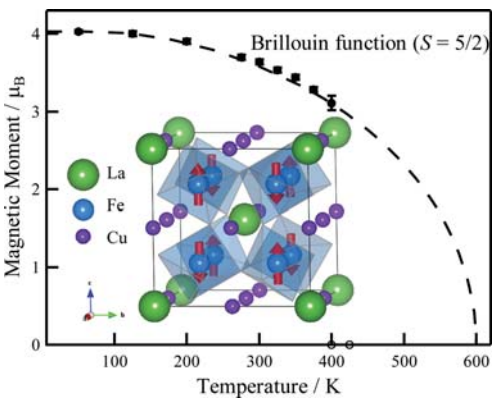

Fig. 3 Temperature dependence of the refined *B*-site Fe^{3+} magnetic moment in $LaCu_3Fe_4O_{12}$. The projected intrinsic Néel temperature of $T_N' \approx 600$ K for the low temperature phase using an $S = 5/2$ Brillouin function is shown. The inset shows the crystal structure and the G-type antiferromagnetic ordering in the low temperature phase. The structure drawing was produced by VESTA.[23]

Recent density functional analysis has suggested that ferrimagnetic ordering of the HT $LaCu^{2+}{}_3Fe^{3.75+}{}_4O_{12}$ state is favored over G-type antiferromagnetic ordering.[26] However no magnetic order of the Cu^{2+} or mixed-valent $Fe^{3.75+}$ spins is observed in the HT phase of $LaCu_3Fe_4O_{12}$ in the neutron data. Magnetic ordering is observed in the related materials $LaCu^{2+}{}_3Mn^{3.75+}{}_4O_{12}$ and $BiCu^{2+}{}_3Mn^{3.75+}{}_4O_{12}$,[5,7] where double exchange between the mixture of d^4 Mn^{3+} and d^3 Mn^{4+} states is pronounced and results in ferromagnetically coupled Mn spins below ~360 K. It should also be noted that materials with unusually high valent Fe cation may undergo simultaneous charge disproportionation and spin ordering as demonstrated in $CaCu_3Fe_4O_{12}$ and $CaFeO_3$, where the transition temperatures are as low as 210 and 290 K, respectively.[16,17] Hence, it seems probable that the intrinsic spin ordering temperature for the $LaCu^{2+}{}_3Fe^{3.75+}{}_4O_{12}$ ground state, T_M, is below the charge transfer transition at T_{CT} = 393 K so that the spin ordered phase is not observed.

4. Conclusions

The present high resolution neutron powder diffraction study has confirmed the initial observations and given more insights into the remarkable properties of $LaCu_3Fe_4O_{12}$ which are dominated by an intermetallic charge transfer transition. Bond valence sums based on accurately determined metal–oxygen bond distances confirm that the charge transfer $3Cu^{2+} + 4Fe^{3.75+} \rightarrow 3Cu^{3+} + 4Fe^{3+}$ at the T_{CT} = 393 K transition occurs completely between two charge states. There is no evidence for substantial valence fluctuations near the first order transition.

G-type antiferromagnetic order of *B*-site Fe^{3+} spins is observed in the LT phase $LaCu^{3+}{}_3Fe^{3+}{}_4O_{12}$ and the thermal evolution of the ordered moment enables an intrinsic $T_N' \approx 600$ K to be estimated although the actual upper limit for the spin order is T_{CT}. No long range magnetic ordering was found in the HT phase, $LaCu^{2+}{}_3Fe^{3.75+}{}_4O_{12}$, showing that any ordering transition in this regime has $T_M < T_{CT}$. Hence, another notable aspect of $LaCu_3Fe_4O_{12}$ is that although its two electronic phases both contain extended networks of magnetic ions, neither shows an intrinsic magnetic transition as the LT phase has $T_N' > T_{CT}$ whereas the HT phase has $T_M < T_{CT}$.

Acknowledgements

We would like to thank Prof. M. Azuma (Institute for Chemical Research, Kyoto University, Japan) for useful discussions. We are also grateful to Mr. M. Senn (CSEC and School of Chemistry, The University of Edinburgh, UK) and Dr E. Suard (Institut Laue-Langevin, Grenoble, France), for their help in the neutron powder diffraction measurements at the Super-D2B diffractometer. This work was supported by the Global COE Program (No. B09), from MEXT, Japan, Grants-in-Aid for Scientific Research (Nos. 19GS0207 and 22740227), and a grant for the Joint Project of Chemical Synthesis Core Research Institutions from MEXT of Japan. The neutron diffraction experiments was done under the Strategic Japanese-UK Cooperative Program by JST/EPSRC. Support was also provided by EPSRC and the Leverhulme Trust, UK.

References

1 Z. Zeng, M. Greenblatt, M. A. Subramanian and M. Croft, *Phys. Rev. Lett.*, 1999, **82**, 3164–3167.
2 A. P. Ramirez, M. A. Subramanian, M. Gardel, G. Blumberg, D. Li, T. Vogt and S. M. Shapiro, *Solid State Commun.*, 2000, **115**, 217–220.
3 M. A. Subramanian, D. Li, N. Duan, B. A. Reisner and A. W. Sleight, *J. Solid State Chem.*, 2000, **151**, 323–325.
4 C. C. Homes, T. Vogt, S. M. Shapiro, S. Wakimoto and A. P. Ramirez, *Science*, 2001, **293**, 673–676.
5 J. A. Alonso, J. Sánchez-Benítez, A. De Andrés, M. J. Martínez-Lope, M. T. Casais and J. L. Martínez, *Appl. Phys. Lett.*, 2003, **83**, 2623–2625.
6 X.-J. Liu, H.-P. Xiang, P. Cai, X.-F. Hao, Z.-J. Wu and J. Meng, *J. Mater. Chem.*, 2006, **16**, 4243–4248.
7 K. Takata, I. Yamada, M. Azuma, M. Takano and Y. Shimakawa, *Phys. Rev. B: Condens. Matter Mater. Phys.*, 2007, **76**, 024429.
8 W. Kobayashi, I. Terasaki, J.-i. Takeya, I. Tsukada and Y. Ando, *J. Phys. Soc. Jpn.*, 2004, **73**, 2373–2376.
9 A. P. Ramirez, G. Lawes, D. Li and M. A. Subramanian, *Solid State Commun.*, 2004, **131**, 251–255.
10 S. Tanaka, N. Shimazui, H. Takatsu, S. Yonezawa and Y. Maeno, *J. Phys. Soc. Jpn.*, 2009, **78**, 024706.
11 Y. W. Long, N. Hayashi, T. Saito, M. Azuma, S. Muranaka and Y. Shimakawa, *Nature*, 2009, **458**, 60–63.
12 Y. W. Long, T. Saito, T. Tohyama, K. Oka, M. Azuma and Y. Shimakawa, *Inorg. Chem.*, 2009, **48**, 8489–8492.
13 A. C. Larson and R. B. Von Dreele, *Los Alamos National Laboratory Report LAUR*, Los Alamos National Laboratory, 2004, pp. 86–748.
14 B. H. Toby, *J. Appl. Crystallogr.*, 2001, **34**, 210–213.
15 I. D. Brown and D. Altermatt, *Acta Crystallogr., Sect. B: Struct. Sci.*, 1985, **41**, 244–247.
16 I. Yamada, K. Takata, N. Hayashi, S. Shinohara, M. Azuma, S. Mori, S. Muranaka, Y. Shimakawa and M. Takano, *Angew. Chem., Int. Ed.*, 2008, **47**, 7032–7035.
17 P. M. Woodward, D. E. Cox, E. Moshopoulou, A. W. Sleight and S. Morimoto, *Phys. Rev. B: Condens. Matter Mater. Phys.*, 2000, **62**, 844–855.
18 K. Imai, M. Koike, H. Takei, H. Sawa, D. Shiomi, K. Nozawa and M. Kinoshita, *J. Phys. Soc. Jpn.*, 1992, **61**, 1819–1820.
19 H. Riesemeier, S. Gärtner, K. Lüders, M. Schmalz and R. Schöllhorn, *J. Phys. Chem. Solids*, 1994, **55**, 613–615.
20 G. A. Costa and E. Kaiser, *Thermochim. Acta*, 1995, **269–270**, 591–598.
21 T. Mizokawa, A. Fujimori, H. Namatame, Y. Takeda and M. Takano, *Phys. Rev. B: Condens. Matter Mater. Phys.*, 1998, **57**, 9550–9556.
22 T. Mizokawa, Y. Morita, T. Sudayama, K. Takubo, I. Yamada, M. Azuma, M. Takano and Y. Shimakawa, *Phys. Rev. B: Condens. Matter Mater. Phys.*, 2009, **80**, 125105.
23 K. Momma and F. Izumi, *J. Appl. Crystallogr.*, 2008, **41**, 653–658.
24 D. Treves, M. Eibschütz and P. Coppens, *Phys. Lett.*, 1965, **18**, 216–217.
25 I. S. Lyubutin, T. V. Dmitrieva and A. S. Stepin, *J. Exp. Theor. Phys.*, 1999, **88**, 590–597.
26 C. Lee, E. Kan and M.-H. Whangbo, 2009, arXiv:0904.4809v1.

